ACS OMEGA

Article

Cite This: ACS Omega 2019, 4, 3745−3754

http://pubs.acs.org/journal/acsodf

Polyethylene Glycol-Modified Layered Double Hydroxides: Synthesis, Characterization, and Study on Adsorption Characteristics for Removal of Acid Orange II from Aqueous Solution

Sujata Mandal,*[,†] Sandhya Kalaivanan,[†] and Asit Baran Mandal[‡,§]

[†]CLRI-Centre for Analysis, Testing, Evaluation & Reporting Services, CSIR-Central Leather Research Institute, Adyar, Chennai 600020, Tamil Nadu, India

[‡]CSIR-Central Leather Research Institute, Adyar, Chennai 600020 Tamil Nadu, India

Supporting Information

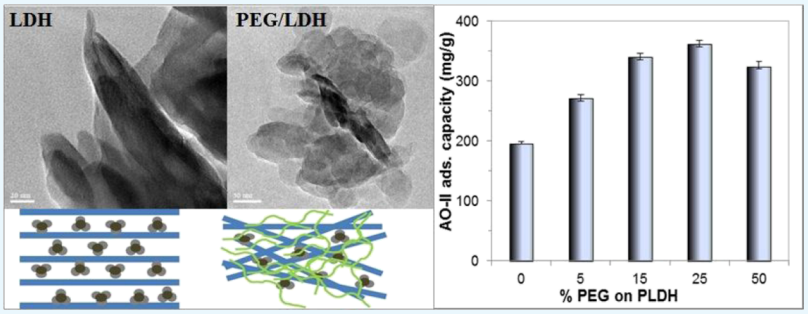

ABSTRACT: The present study aimed to improve the adsorption characteristics of the pristine layered double hydroxide (LDH) by physicochemical modification using polyethylene glycol (PEG_{400}), a nontoxic hydrophilic polymer. With this objective, LDH was synthesized and modified with different concentrations of PEG_{400}. The PEG-modified LDHs (LDH/PEGs) were characterized using X-ray diffraction, thermogravimetric analysis, Brunauer−Emmett−Teller surface area and porosity measurement, scanning electron microscopy, transmission electron microscopy, Fourier transform infrared spectroscopy, and zeta potential measurements. The adsorption properties of the pristine LDH (PLDH) and the LDH/PEGs were studied for the removal of Acid Orange II from water, and the results were compared. The PLDH treated with 15% PEG solution showed ∼30% increase in adsorption capacity as compared to the PLDH. The adsorption isotherm data were analyzed using Langmuir, Freundlich, and Temkin isotherm models. The values of thermodynamic parameters such as ΔS and ΔH showed the spontaneous and endothermic nature of the adsorption process. The adsorption kinetics data for both PLDH and the LDH/PEG adsorbents presented a good fit to the pseudo-second-order kinetic model.

1. INTRODUCTION

Dyes are the most significant contaminant among various industrial pollutants. Several dyes and their decomposition products are toxic to living organisms and are generally not removed from wastewater by conventional wastewater treatment systems. Therefore, excessive use of dyes/colorants has largely contributed to the environmental pollution. A number of technologies have been developed and implemented for the purpose of removing dye/colorants from wastewater,[1−3] including adsorption,[4] coagulation/flocculation,[5] advanced oxidation processes,[6] membrane-based technologies,[7] and biological treatment processes.[8] However, among these methods, adsorption has become one of the most effective and low-cost methods for removing dyes/colorants from wastewater.[4] A wide spectrum of adsorbents, such as carbon-based materials,[9] clay and its composites,[10,11] waste material,[12] natural/synthetic polymers,[13] magnetic materials,[14] inorganic nanomaterials,[15] functionalized MOFs,[16] and so forth, have been explored for this purpose. In order to achieve the desired water quality and for a sustainable water treatment technology, a careful selection of adsorbents is paramount.

Layered double hydroxides (LDHs), also named as hydrotalcite-like compounds, are a family of inorganic layered materials with positively charged metal hydroxide layers and interlayer balancing anions.[17] Because of the presence of large interlayer spaces and a reasonable number of exchangeable anions, they act as potential ion exchangers/adsorbents.[18,19] Interactions of polymer molecules with the LDH structure forming LDH/polymer (nano)composites with interesting physical and chemical properties are being explored for various applications by several research groups.[20−22] In the recent decade, an increasing number of reports on synthesis and application of various LDH/polymer (nano)composites shows

Received: October 10, 2018
Accepted: December 26, 2018
Published: February 20, 2019

DOI: 10.1021/acsomega.8b02743
ACS Omega 2019, 4, 3745−3754

that these materials have promising future; however, application of these materials in water treatment is limited.

In the present study, polyethylene glycol (PEG_{400}), a nontoxic hydrophilic polymer, has been explored for physicochemical modification of Mg/Al LDH (Mg/Al molar ratio 2) with the aim to increase the adsorption performance of the LDH. The present communication reports synthesis of PEG-modified LDHs with varying concentrations of PEG_{400}, their physicochemical characterization and adsorption behavior for the azo dye, Acid Orange II (AO-II) in aqueous medium. The influence of various parameters such as concentration of PEG used, adsorption temperature, initial dye concentration, contact/adsorption time, and solution pH, on the dye adsorption characteristics of the LDH/PEG is systematically investigated.

2. RESULTS AND DISCUSSIONS

2.1. Characterization. Chemical analysis results of the pristine LDH (PLDH) and LDH/PEGs (Table 1) show that

Table 1. Chemical Compositions of the PLDH and LDH/PEG Adsorbents

adsorbent	Mg (%)	Al (%)	C (%)	H (%)	N (%)
PLDH	15.08	8.32	0.28	2.65	5.01
LDH/PEG-5	13.73	6.78	4.23	2.90	4.82
LDH/PEG-15	14.83	7.95	3.75	2.78	4.76
LDH/PEG-25	10.54	5.82	6.21	3.30	3.90
LDH/PEG-50	10.32	5.65	5.96	3.22	3.82

all the adsorbents exhibit a Mg/Al molar ratio close to two. The carbon content in the adsorbents increased in the order PLDH < LDH/PEG-15 < LDH/PEG-25 which indicates attachment of more PEG molecules with the PLDH on increase in the PEG concentration. The traces of carbon detected in the PLDH may be due to the absorption of atmospheric carbon dioxide during synthesis. The occurrence of nitrogen in the PLDH and in the LDH/PEG is due to the presence of surface and interstitial nitrate ions from the precursor salts. The nitrogen content in the LDH/PEG decreased with increase in the PEG concentration, which indicates that more and more nitrate ions of the PLDH are exchanged by the PEG_{400} during reaction.

The X-ray diffraction patterns of the PLDH and LDH/PEGs presented in Figure 1 exhibit the X-ray diffraction (XRD) patterns typical of synthetic LDHs. The XRD patterns show

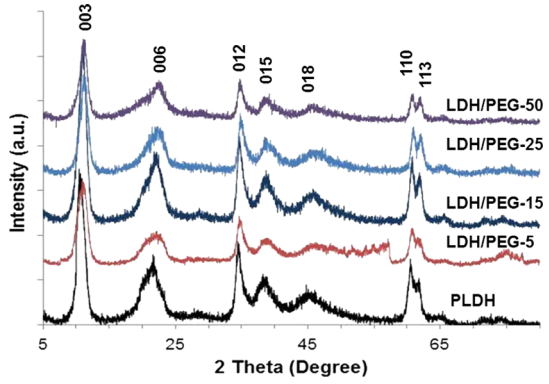

Figure 1. X-ray diffraction patterns of the PLDH and the LDH/PEG adsorbents.

sharp and pointed diffraction peaks at 2θ positions 10.8, 21.6, 34.5, 38.4, 45.1, 60.6, and 61.8° due to the 003, 006, 012, 015, 018, 110, and 113 diffraction planes, respectively.[23] The unit cell parameters, c and a, estimated from the positions of the (003) ($c = 3d_{003}$) and (110) ($a = 2d_{110}$) reflections are 2.46 and 0.305 nm, respectively. These values agree with those reported in the literature for Mg/Al LDHs with nitrate as interlayer anions and having a Mg/Al molar ratio close to 2.[19] The values of basal spacing (d_{003}) for the PLDH, LDH/PEG-5, LDH/PEG-15, LDH/PEG-25, and LDH/PEG-50 are 0.820, 0.797, 0.798, 0.797, and 0.785 nm, respectively. The close values of basal spacing of the PLDH and the LDH/PEGs show no significant change in the basic crystal structure of the LDH on treatment with PEG_{400}. The sharp peaks signify the high crystalline nature of the LDH/PEGs similar to that of the PLDH.

The thermogravimetric analysis (TGA) curves of the PLDH and LDH/PEGs generally show decrease in residual mass with increase in the PEG concentration in the composites (Figure 2). The TG curve of the PLDH is divided into two mass loss

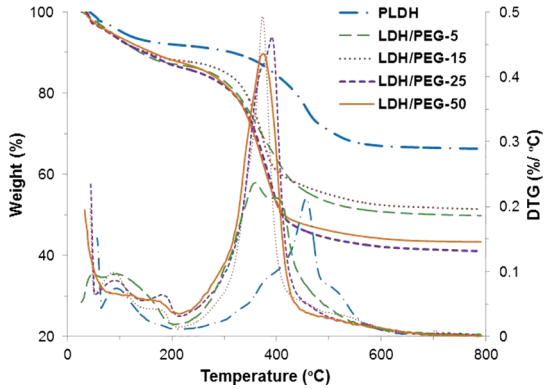

Figure 2. TGA and derivative TGA (DTG) profiles of the PLDH and LDH/PEG adsorbents.

steps. The weight loss below 150 °C is ca. 6.2% and is attributed mainly to the loss of physically adsorbed water molecules. In the second step between 300 and 550 °C, the weight loss is ca. 26%, resulting from the dehydroxylation and elimination of intercalated ions and water molecules, after which the LDH loses its characteristic layered structure.[24] The weight loss in the LDH/PEGs took place primarily in two steps, as marked by the exothermic peaks in the DTG curves, between 50 to 210 and 210 to 500 °C.

The weight loss between 50 and 210 °C is due to the loss of physisorbed water molecules and the decomposition of free PEG molecules. The larger mass loss of approximately 33 to 42% of the total mass appeared in the temperature range 210–500 °C for the LDH/PEGs corresponding to the decomposition of PEG molecules, dehydroxylation, and elimination of intercalated anions. The TGA data indicate relatively lower thermal stability of the layered structure of the LDH/PEGs than that of the PLDH. The total weight loss recorded at 800 °C for the PLDH, LDH/PEG-5, LDH/PEG-15, LDH/PEG-25, and LDH/PEG-50 are 33.7, 50.2, 48.6, 58.9, and 56.7%, respectively.

The scanning electron microscopic (SEM) images of the PLDH and LDH/PEG-15 show flake-like particles having an average dimension less than 100 nm (Figure 3a,b). Figure 3 clearly shows that the stacked particles of PLDH (Figure 3a)

DOI: 10.1021/acsomega.8b02743
ACS Omega 2019, 4, 3745−3754

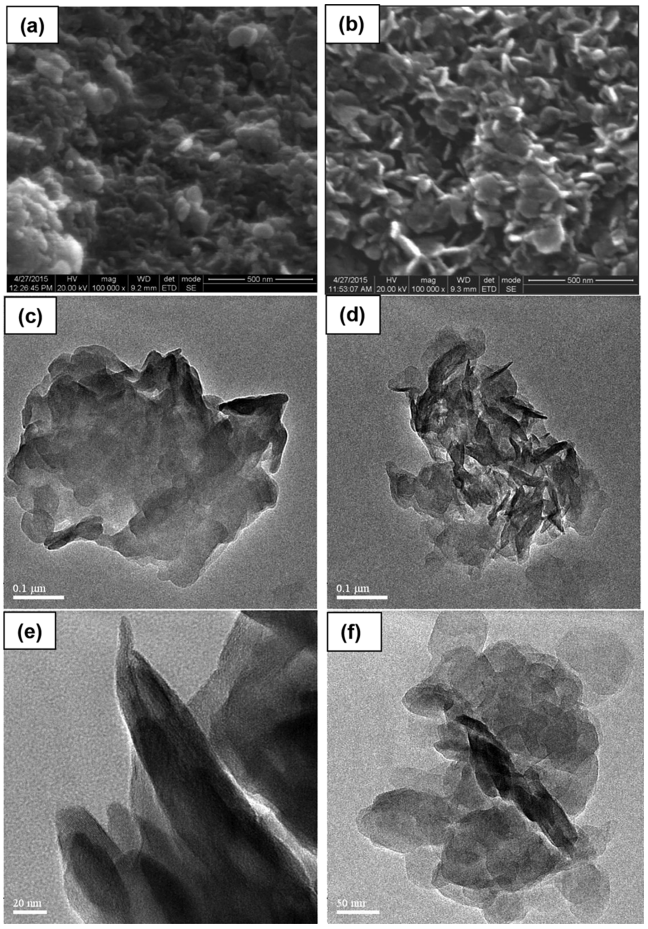

Figure 3. SEM images (a,b) and TEM images (c–f) of the (a,c,e) PLDH and (b,d,f) LDH/PEG-15.

got exfoliated in the LDH/PEG-15 (Figure 3b) after treatment with PEG_{400}. The transmission electron microscopic (TEM) images (Figure 3c–f) show the hexagonal flake-like particles of the adsorbent having a dimension between 50 and 80 nm. TEM images clearly show the agglomerated particles in PLDH (Figure 3c,e), whereas dispersed particles in LDH/PEG-15 (Figure 3d,f).

The specific surface areas of PLDH and LDH/PEG-15 are 101.2 and 107.9 m^2/g, respectively, while the total pore volumes of both PLDH and LDH/PEG-15 are the same (0.22 cc/g). The identical shape of the nitrogen adsorption–desorption isotherms for the PLDH and LDH/PEG-15 (Figure S1) indicates that the pore structures of the two adsorbents are analogous. The adsorption hysteresis relates to the type IV isotherm of the IUPAC classification of physisorption which are characteristics of the mesoporous materials.[25] The BJH desorption curves (Figure S1) show two different pore sizes (2.3 and 3.5 nm) of the PLDH, which merged into one (3.5 nm) in LDH/PEG-15. This indicates that the relatively smaller pores of the PLDH are filled with the PEG in LDH/PEG-15. The high surface area, mesoporous nature, and nano-size pores signify good adsorption characteristics of these adsorbents.

The zeta potential (ζ) is an important parameter to evaluate the surface charge and dispersity of an adsorbent. The zeta potential (ζ) values of the PLDH, LDH/PEG-15, LDH/PEG-25, and LDH/PEG-50 in water are 35.9 ± 2.1, 37.3 ± 1.4, 37.1 ± 1.1, and 37.9 ± 0.5 mV, respectively. The zeta potential values indicate that no chemical interaction takes place between PLDH and PEG_{400} under the reaction conditions of the present study.

2.2. Influence of the PEG_{400} Concentration on Dye Removal. Adsorption of AO-II by the LDH/PEGs prepared using different PEG_{400} concentrations is compared with that of the PLDH in Figure 4 (0% PEG represents PLDH). The

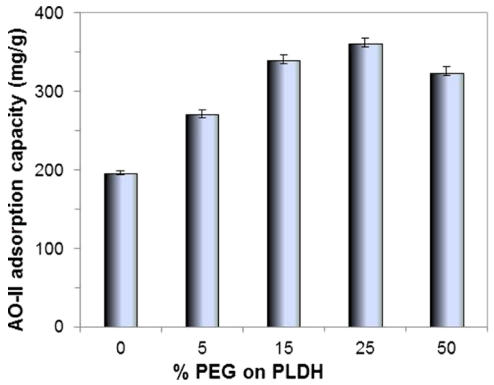

Figure 4. Influence of the PEG_{400} concentration on the AO-II adsorption capacity of the LDH/PEG adsorbents (initial AO-II concentration: 200 mg/L, amount of the adsorbent: 0.5 g/L, contact time: 6 h, temperature: 30 °C).

LDH/PEGs invariably show higher dye adsorption capacity than that of the PLDH, while PEG_{400} itself has no competence for AO-II adsorption–decomposition. Nevertheless, the concentration of PEG_{400} used for making LDH/PEGs has significant influence on their adsorption capacity. An increase in the PEG_{400} concentration from 5 to 25% leads to an enhanced adsorption capacity; however, a further increase in the PEG_{400} concentration above 25% has a detrimental effect on the adsorption capacity. Yet, the increase in adsorption capacity from LDH/PEG-15 to LDH/PEG-25 is marginal with respect to the increase in the PEG_{400} concentration. Hence, a detailed adsorption study was performed using LDH/PEG-15 and the results were compared with those of the PLDH.

2.3. Adsorption Kinetics. The decrease in the AO-II concentration as a function of reaction time at two different concentrations of AO-II for the PLDH and the LDH/PEG-15 is presented in Figure 5. A large decrease in the AO-II concentration indicates better adsorption capacity of the LDH/PEG-15. The improvement in adsorption capacity in

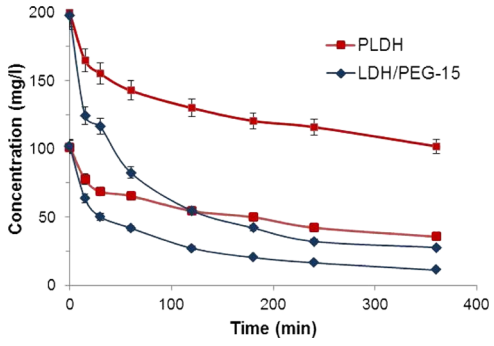

Figure 5. AO-II adsorption kinetics of the PLDH and the LDH/PEG-15 at two different concentrations of AO-II (AO-II concentration: 100 and 200 mg/L, amount of the adsorbent: 0.5 g/L, contact time: 0–6 h, temperature: 30 °C).

DOI: 10.1021/acsomega.8b02743
ACS Omega 2019, 4, 3745–3754

LDH/PEG-15 is more pronounced in the higher AO-II concentration. The adsorption of AO-II by the PLDH and LDH/PEG-15 are 48.9 and 86%, respectively, when the initial concentration of AO-II is 200 mg/L. The kinetic data were fitted to a pseudo-second-order kinetic model proposed by Ho and McKay.[26] The pseudo-second-order kinetic equation is given below

$$\frac{t}{q_t} = \frac{1}{k_2 q_e^{\,2}} + \frac{t}{q_e} \quad (1)$$

where t is the time in minutes, q_t is the amount of adsorbate per unit gram of the adsorbent at time t, q_e has the same meaning as mentioned in previous section, and k_2 is the pseudo second-order rate constant.

The pseudo-second-order kinetic constants calculated from the slope and intercept of the linearized plot of the eq 1 (Figure S2) are presented in Table 2 along with their correlation coefficients.

Table 2. Pseudo Second-Order Kinetic Constants for AO-II Adsorption on PLDH and LDH/PEG-15

adsorbent	C_0 (mg/L)	$q_{e,exp}$ (mg/g)	pseudo second-order model		
			$q_{e,cal}$ (mg/g)	k_2 [g/(mg·min)]	R^2
PLDH	100	131.5	142.8	1.43×10^{-4}	0.98
	200	195.3	212.8	0.97×10^{-4}	0.99
LDH/PEG-15	100	181.8	196.1	1.65×10^{-4}	0.99
	200	339.6	370.4	0.82×10^{-4}	0.99

The values of the correlation coefficient (R^2) indicate excellent fitting of the kinetic data with the pseudo-second-order kinetic model. The value of the second-order rate constant (k_2) decreased with an increase in the initial dye concentration. Reports from other research groups also proposed the pseudo-second-order kinetic model as the suitable model for adsorption of dyes on pristine and calcined LDHs.[23,27] This result indicates a strong interaction between the AO-II and the adsorbents.[27]

2.4. Adsorption Isotherm. The influence of the initial AO-II concentration on the adsorption capacity of the adsorbents was studied at three different temperatures, 30, 40, and 50 °C, and by varying the initial AO-II concentration from 200 to 800 mg/L (Figure S3). The equilibrium adsorption capacities increased with increase in the initial AO-II concentration and with increase in temperature. At all the reaction temperatures, the adsorption capacity of LDH/PEG-15 is much higher than that of the PLDH.

The equilibrium adsorption data were fitted to the Langmuir,[28] Freundlich,[29] and Temkin,[30] isotherm models. The linearized form of the Langmuir (eq 2), Freundlich (eq 3), and Temkin (eq 4) isotherm models used in the present study is given below

$$\frac{C_e}{q_e} = \frac{1}{b_L V_m} + \frac{C_e}{V_m} \quad (2)$$

where C_e and q_e have the same meaning as mentioned in the previous section, and b_L and V_m are Langmuir isotherm constants representing respectively adsorption bond energy and monolayer adsorption capacity.

$$\ln q_e = \ln k + \frac{1}{n} \ln C_e \quad (3)$$

where n and k are Freundlich isotherm constants. The constant n represents adsorption intensity and k represents adsorption capacity.

$$q_e = \frac{RT}{b_T} \ln A + \frac{RT}{b_T} \ln C_e \quad (4)$$

and $B = RT/b_T$, where B is a constant related to the heat of adsorption, A is the equilibrium binding constant (L/mg), R is the universal gas constant (8.314 J/mol/K), and T is the temperature in absolute scale (K).

The values of isotherm constants for each isotherm model were determined from the slope and intercept of the linearized plot of the respective isotherm equations. The values of various isotherm constants and their corresponding correlation coefficients (R^2) at three different experimental temperatures are listed in Table 3. The values of Langmuir constant V_m, representing monolayer adsorption capacity, for both PLDH and LDH/PEG-15 are very close to those of the experimental values. Nevertheless, the AO-II adsorption capacity of the LDH/PEG-15 is much higher than that of the PLDH. The monolayer adsorption capacity of AO-II on the PLDH and the LDH/PEG-15 at 30 °C is 490.2 and 625.0 mg/g, respectively. The low values of the Langmuir constant b_L, representing adsorption bond energy, indicate the physical nature of the adsorption of AO-II on PLDH and LDH/PEG-15. The values of the Freundlich constant n greater than one (>1) represents good adsorption characteristics of the LDH/PEG-15 for the adsorption of AO-II.[31] The values of correlation coefficients

Table 3. Values of the Isotherm Constants and Their Correlation Coefficients at Different Temperatures

		isotherm constants at different temperatures					
		PLDH			LDH/PEG-15		
isotherm models	constants	30 °C	40 °C	50 °C	30 °C	40 °C	50 °C
Langmuir	b_L	0.003	0.012	0.010	0.052	0.036	0.040
	V_m	490.20	442.48	555.56	625.00	714.28	724.64
	R^2	0.938	0.993	0.985	0.981	0.981	0.950
Freundlich	n	1.85	2.92	2.49	3.45	4.54	4.20
	k	10.83	47.86	40.89	124.96	186.98	179.29
	R^2	0.922	0.906	0.844	0.997	0.973	0.892
Temkin	A	0.03	0.01	0.08	0.93	1.73	1.53
	B	116.90	94.34	127.4	106.67	102.92	109.95
	R^2	0.903	0.925	0.868	0.890	0.979	0.850

DOI: 10.1021/acsomega.8b02743
ACS Omega 2019, 4, 3745−3754

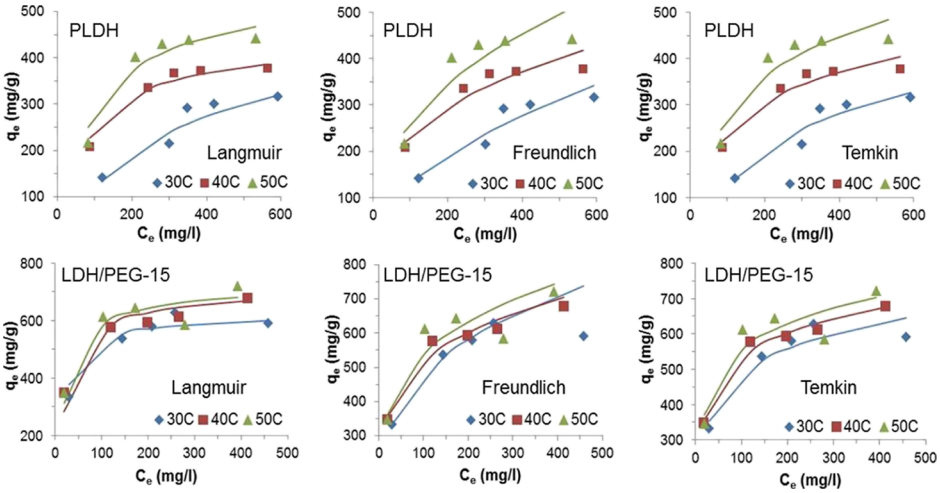

Figure 6. AO-II adsorption isotherms of PLDH and LDH/PEG-15 in water at different temperatures obtained using Langmuir, Freundlich, and Temkin isotherm models (the data points indicate experimental values and the solid lines indicate model fittings).

Table 4. Comparison of AO-II Adsorption Capacities of Various Adsorbents

adsorbent	adsorption capacity from Langmuir adsorption model (mg/g)	initial dye concentration (mg/L)	contact time	refs
Mg/Al LDH	224	50	3 days	23
calcined Mg/Al LDH	602			
Mg/Al-LDH-NO_3	947.1[a]	7−1052	200 min	27
LDHs of compositions, Mg/Al, Cu/Al, Co/Al, Mg/Cu/Al, Mg/Co/Al, and Co/Cu/Al	59.2−129.8	100−300	240 min	32
zirconium based chitosan microcomposite adsorbent	926	50−300 at pH 2	600 min	33
acid and basic functionalised titanosilicate	98 and 49	50−350	30 min	34
activated carbon	329	300−2100	300 min	35
mesoporous carbon CMK-3	385			
ammonia tailored CMK-3	596			
Mg/Al HT cal	634.4	0−5016	24 h	36
HT macro cal	1521.2			
LDH/PEG-15	625.0	100−800	120 min	present work

[a]Value taken from the equilibrium adsorption study.

indicate suitability of the Langmuir isotherm model for the present adsorbent−adsorbate system.

The plots of adsorption isotherms obtained using the values of constants from linearized plots of the Langmuir, Freundlich, and Temkin isotherm models, and the experimental isotherm data are presented in Figure 6. The q_e value for each isotherm model was calculated using the isotherm constants from Table 3 and the respective isotherm equations. In the Langmuir isotherm, the experimental isotherm data (data points) fitted reasonably well with the isotherm model (solid lines) over the wide range of concentration and in all the three experimental temperatures. In the case of the Freundlich isotherm, the experimental isotherm data and the isotherm model are in good agreement in the lower concentrations but deviate more and more with the increase in the adsorbate concentration. The Temkin isotherm model fails to provide the realistic adsorption capacity value and hence cannot be utilized for the present adsorbent−adsorbate system. Hence, the Langmuir isotherm model can be considered as the most suitable model for AO-II adsorption on PLDH and LDH/PEG adsorbents.

To evaluate the AO-II adsorption performance of the LDH/PEG-15, the adsorption capacity value from the present study was compared to that of the other reported adsorbent materials and is summarized in Table 4. The reaction conditions like initial dye concentration and contact time are also included in Table 4 for proper assessment.

The data in Table 4 show that our adsorbents exhibit good adsorption capacities at reasonably high initial dye concentrations. Moreover, the time taken to achieve this adsorption capacity value by the LDH/PEG-15 is much less than that for the other reported adsorbents. The reaction/contact time is an important parameter for feasibility of any real-life water treatment system. The less the contact time, the more is the efficiency of the water treatment system. Hence, in terms of adsorption capacity and contact time, the present LDH/PEG-15 adsorbent is exceptional to the other adsorbents reported for removal of AO-II dye from water.

2.5. Adsorption Thermodynamics. In order to understand the thermodynamic nature of the present adsorbent−adsorbate system at varying temperatures, thermodynamic parameters such as the change in Gibbs free energy (ΔG), enthalpy (ΔH), and entropy (ΔS) were calculated using the following equations

$$\ln K_d = \frac{\Delta S}{R} - \frac{\Delta H}{RT} \quad (5)$$

$$\Delta G = -RT \ln K_d \quad (6)$$

DOI: 10.1021/acsomega.8b02743
ACS Omega 2019, 4, 3745−3754

Table 5. Values of the Thermodynamic Parameters for Adsorption of AO-II on LDH/PEG-15

adsorbent	ΔH kJ/mol	ΔS J/mol/K	$-\Delta G$ (kJ/mol)		
			30 °C	40 °C	50 °C
LDH/PEG-15	11.90 ± 0.21	0.10 ± 0.002	17.28 ± 0.15	18.24 ± 0.11	19.20 ± 0.18

where $K_d = q_e/C_e$, R is the universal gas constant (8.314 J/mol/K), T is the temperature in absolute scale (K), and K_d is the adsorption distribution co-efficient (L/g).

The values of ΔH and ΔS were calculated from the slope and intercepts of the van't Hoff plot for $\ln(K_d)$ versus $1/T$ (Figure S4) and are presented in Table 5. The value of ΔH (<80 kJ/mol) signifies the physical nature of the present adsorption process. The positive value of ΔH and ΔS indicates endothermic nature and spontaneity of the present adsorbent−adsorbate system. The negative value of the free energy (ΔG), which again decreased with increase in temperature, indicates that the adsorption process is feasible and thermodynamically spontaneous at higher temperatures. Similar results were reported by Li et al. (2009) for the adsorption of 2-nitroaniline onto activated carbon prepared from cotton stalk fiber.[37]

2.6. Influence of Solution pH. The influence of solution pH on the AO-II adsorption by the LDH/PEG-15 was studied in the solution pH range between 2 and 10. The AO-II adsorption capacity of LDH/PEG-15 changed between 230.5 and 333.5 mg/g on varying the solution pH between 2.1 and 10 (Figure S5). The adsorption capacities are not significantly affected by the solution pH between 4 and 9.1. However, the maximum adsorption was achieved at the normal pH of the AO-II solution (pH ≈ 6.2). The slight decrease in adsorption capacity at pH < 4 may be due to the dissolution of the metal hydroxides of the adsorbents in the acidic solution. The observed decrease in adsorption capacity on moving toward the alkaline medium may be due to the increase in the concentration of the competitive hydroxyl ion (OH^-) in the solution. It is interesting to observe that the equilibrium pH values of the solutions recorded after 2 h of adsorption are between 6.1 and 7.9, though the initial pH values of the solutions were between 3 and 9.1. This kind of buffering action of the LDH has been previously observed and reported by our research group.[38] The present study reveals that the buffering property of the PLDH is retained even in the LDH/PEG-15.

2.7. Desorption and Regeneration Studies. Desorption of AO-II from the AO-II adsorbed LDH/PEG-15 in the alkaline and neutral aqueous medium was studied at 28 °C as a function of time, and the results are presented in Figure 7a. After 24 h of contact, a maximum of 22.6 and 5.1% desorption was observed in 0.05 M NaOH solution and in water, respectively. The low desorption of AO-II from the adsorbent is attributed to the confinement of the AO-II in the interlayer space of the layered structure.

Regeneration of an adsorbent is practically important for its re-use in removing pollutants from water. Because of the very low desorption of AO-II in the alkaline medium, the regeneration of the adsorbent was tested by thermal treatment instead of the chemical method. Adsorption studies were performed using the thermally regenerated[23] adsorbent LDH/PEG-15 for four cycles (R_1 to R_4), and the results are presented in Figure 7b. R_0 represents the adsorption by fresh adsorbents. Figure 7b shows that there is ∼18% loss in adsorption capacity in the first regeneration cycle after which there is not much decrease in the adsorption capacity up to the fourth regeneration cycles. These results reveal that the thermal regeneration of the used adsorbent is feasible at least up to first four cycles.

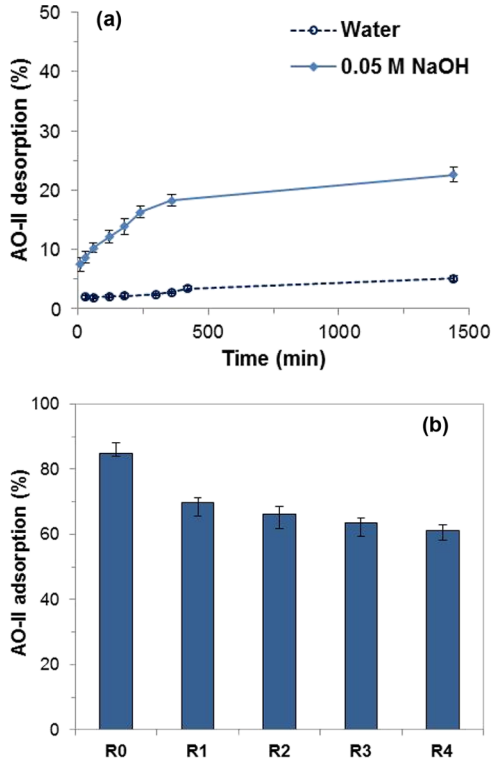

Figure 7. (a) Desorption of AO-II from the AO-II-adsorbed LDH/PEG-15 in the alkaline and neutral aqueous medium at 28 °C as a function of time and (b) AO-II adsorption on the fresh and the regenerated LDH/PEG-15.

2.8. Mechanism of AO-II Uptake by the LDH/PEG Adsorbent. Although there is no significant difference in the crystal structure, surface area, and porosity between the PLDH and the LDH/PEG-15 adsorbents, the remarkable increase in the adsorption capacity of the PLDH on treatment with PEG_{400} needs further elucidation. To understand the AO-II adsorption mechanism of the PLDH and LDH/PEG-15 adsorbents, the AO-II-loaded adsorbents (800 mg/L AO-II) were collected, washed, and dried, after which FTIR spectra and XRD patterns of the samples were recorded. Figure 8 shows the XRD patterns and Fourier transform infrared (FTIR) spectra of the adsorbents recorded before and after adsorption.

The XRD patterns of the AO-II-loaded adsorbents were recorded in the 2θ range from 2 to 32° and compared with that of the PLDH in Figure 8a. The two harmonic peaks at 2θ positions 10.6 and 21.7° (in PLDH) correspond to the d-spacings 0.82 and 0.41 nm, respectively, are characteristic of an LDH with a nitrate interlayer ion. However, in the XRD patterns of the AO-II-loaded adsorbents, the peaks due to 003 and 006 diffraction planes corresponding to nitrate ions disappeared and new peaks appeared at 2θ positions 3.9 and 7.9° with the d-spacings 2.22 and 1.11 nm, respectively. The increase in d-spacing from 0.82 nm (before adsorption) to 2.22

DOI: 10.1021/acsomega.8b02743
ACS Omega 2019, 4, 3745−3754

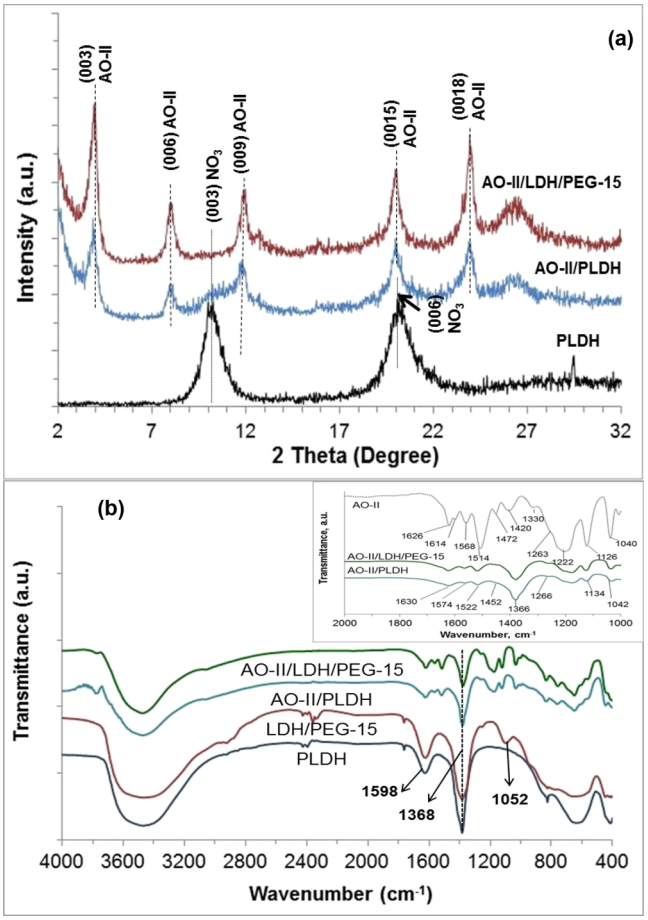

Figure 8. (a) XRD patterns of the AO-II-loaded adsorbents and (b) FTIR spectra of the adsorbents before and after adsorption. The inset of figure (b) shows the amplified FTIR spectrum between 1000 and 2000 cm^{-1}.

nm (after adsorption) indicates intercalation of AO-II ions within the LDH's galleries of both PLDH and LDH/PEG-15. The XRD results are in agreement with those reported for the adsorption of AO-II on LDHs.[27,39]

The FTIR spectra of the PLDH and LDH/PEG-15 taken before and after adsorption of AO-II are presented in Figure 8b. The intense and broad absorption band between 3700 and 3000 cm^{-1}, in the spectra of all the samples is due to the stretching vibrations of the hydrogen-bonded hydroxyl groups in the metal hydroxide sheets. The antisymmetric stretching vibration of the nitrate ions intercalated in the interlayer space of the adsorbents is shown by the sharp peak between 1380 and 1330 cm^{-1}. The absorption band at 1368 cm^{-1} also accounts for the stretching vibration of carbonate ions present in small amounts.[40] The medium sharp peak at 1598 cm^{-1} is due to the O−H bending vibration of the interlayer water molecules.[41] The LDH/PEG-15 shows three additional peaks at 1052, 1203, and 2867 cm^{-1} which are characteristic peaks for bending vibration of the C−O−H group and symmetric stretching vibration of the C−H group due to the PEG.[42] The FTIR spectra of the AO-II-loaded PLDH and LDH/PEG-15 are alike which indicates that the AO-II uptake mechanisms of these two adsorbents are the same. The inset of Figure 8b shows characteristic absorption bands of AO-II at 1626 (or 1630) cm^{-1} and 1514 (or 1506) cm^{-1} for the aromatic C═C and azo group (−N═N−), respectively.[43] The absorption bands due to the coupling between the benzene mode and SO_3^- group can be seen at 1126 (or 1134) cm^{-1} and 1040 (or 1042) cm^{-1}.[43] Intercalation of AO-II in the interlayer space of the adsorbents does not significantly affect the characteristic vibration bands of AO-II. This observation confirms that the present dye uptake process is purely a physical adsorption.

The particle size distribution of PLDH in aqueous medium studied by the dynamic light scattering experiment shows polydispersity of the LDH and the *z*-average diameter is 216.8 nm (Figure S6). The same experiment with LDH/PEG-15 and LDH/PEG-50 shows a very different nature of dispersity of the two adsorbents. While LDH/PEG-15 shows better dispersity than the PLDH with the *z*-average diameter being 160.8 nm (Figure S7), which is close to the average diameter obtained from SEM study, the dispersity of LDH/PEG-50 is low with the *z*-average diameter being 218.8 nm (Figure S8). This result implies that treatment of LDH with the high concentration of PEG has a detrimental effect on its dispersity. In other words, the agglomeration of the LDH particles is reduced on treatment with a specific range of concentration of PEG_{400}, which in turn increased the adsorption capacity by increasing the available active sites of the adsorbent to the adsorbate. A schematic of the plausible AO-II uptake mechanism of the LDH/PEG-15 is presented in Scheme 1. A review of literature

Scheme 1. Schematic Diagram of the AO-II Uptake Mechanism by the PEG-Treated LDH

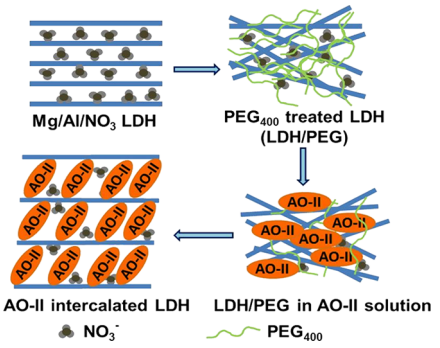

reports, unlike the high-molecular weight PEGs, the low-molecular weight PEGs do not react with the LDH but act as a dispersing agent and reduce aggregation of LDH particles in aqueous medium.[44] Therefore, the significant increase in adsorption capacity of the LDH on treatment with PEG_{400} may be attributed to the better dispersion and/or reduced agglomeration of the adsorbent particles.

3. CONCLUSIONS

In summary, Mg/Al/NO_3 LDHs were synthesized and modified with PEG_{400}. The influence of PEG on physicochemical characteristics and adsorption properties of the LDH/PEG adsorbents was studied. Both the pristine and the PEG-modified LDHs (PLDH and LDH/PEG-15) exhibited reasonably high surface area, mesoporous nature, and positive zeta potential values, which are characteristics of good adsorbents. The AO-II adsorption capacities of the PLDH and the LDH/PEG-15 were 490.2 and 625.0 mg/g, respectively. AO-II adsorption capacity of the PLDH increased by about 30% on treatment with PEG_{400}. Compared to many reported adsorbents, the LDH/PEG adsorbents exhibited remarkable high adsorption capacity and adsorption rate for

DOI: 10.1021/acsomega.8b02743
ACS Omega 2019, 4, 3745−3754

the anionic dye AO-II. The thermodynamics parameters like ΔH, ΔG, and ΔS indicated endothermic, physical, spontaneous and feasibility of the present adsorbent−adsorbate system. The pseudo-second-order kinetic model and the Langmuir isotherm models are most suitable to explain the experimental adsorption data. The AO-II uptake by the adsorbents was primarily via electrostatic interactions between the positively charged metal hydroxide layers and the anionic chromophores of AO-II, and the intercalation of the AO-II into the interlayer space between the metal hydroxide layers. However, the enhanced adsorption capacity of the PEG-modified LDH is mainly due to the better dispersity of the LDH/PEG as compared to the PLDH. Owing to the high adsorption capacity of the LDH/PEGs and nontoxic nature of both LDH and PEG_{400}, they can be potential adsorbent for water/wastewater treatment.

4. MATERIALS AND METHODS

4.1. Reagents. Magnesium nitrate hexahydrate, aluminium nitrate nonahydrate, and PEG_{400} were procured from MERCK Chemicals. Sodium hydroxide pellets (AR grade) were purchased from Himedia laboratories. AO-II Sodium Salt (C.I. no. 15510, molecular weight 350.32, λ_{max} 483 nm) was procured from Sigma-Aldrich. Double distilled water was used for all the experiments and for the preparation of standard solutions.

4.2. Synthesis of the Adsorbents. *4.2.1. Synthesis of Mg/Al LDH.* The Mg/Al LDH was prepared via the co-precipitation method, and the detailed process is described in our previous publication.[45] A solution containing the mixture of magnesium and aluminium nitrates (Mg/Al molar ratio 2) was co-precipitated in an aqueous medium using 2 M NaOH solution at 60 °C and at a pH of 10 ± 0.5. The precipitate thus formed was aged for 16 h in the reaction mixture under continuous stirring after which the precipitate was separated by centrifugation. The solid mass thus obtained was washed thoroughly with distilled water to remove any excess alkali and dried at 60 °C in an air oven and powdered. The solid thus obtained is hereafter denoted as PLDH.

4.2.2. Synthesis of the PEG Modified LDH (LDH/PEG) Adsorbents. The PEG-modified LDHs were synthesized by a slightly modified method as described by Gunister et al. in 2013 for the synthesis of the poly (diallyldimethylammonium-chloride)/sodium-montmorillonite composite.[46] A fixed amount of the PLDH was reacted with an aqueous solution of PEG_{400} at 50 °C for 4 h. The LDH/PEG thus formed was separated from the solution by centrifugation, dried at 50 °C in an air oven, and powdered. A series of LDH/PEG adsorbents were prepared by varying the concentration of the PEG_{400} solution between 0 and 50% (w/v). The LDH/PEG adsorbents thus prepared by using 5, 15, 25, and 50% aqueous solution of PEG_{400} were named as LDH/PEG-5, LDH/PEG-15, LDH/PEG-25, and LDH/PEG-50, respectively.

4.3. Characterization Techniques. The synthesized PLDH and the LDH/PEG adsorbents were characterized for their chemical composition and physical behavior using different techniques. The XRD patterns of the adsorbents were recorded by X'Pert-PRO XRD from PANalytical Instruments using Cu Kα radiation. The FTIR spectra of the adsorbents were recorded in a Cary 600 FTIR spectrometer (Agilent Technologies Pvt. Ltd, USA) by the KBr pellet method. The thermal analyses were performed by a thermogravimetric analyzer (model Q50 from TA Instruments, Austria) in the temperature range from room temperature to 800 °C with a ramping rate of 20 °C/min. The surface morphologies of the adsorbents were studied using SEM (FEI Quanta 200 SEM). The concentrations of magnesium and aluminium in the adsorbents were determined using inductively coupled plasma−optical emission spectroscopy (model: Prodigy, Teledyne Leeman Labs, USA). The C, H, and N present in the adsorbents were analyzed using the CHNS analyzer (Elementar Vario Micro Superuser, Germany). The Brunauer−Emmett−Teller surface area and porosity of the adsorbents were measured by the nitrogen adsorption−desorption technique at 77 K using a surface area analyzer (model: Autosorb 1, Quantachrome Instruments, USA). The zeta potential (ζ) and particle size distribution of the adsorbents were measured by the dynamic light scattering technique after dispersing the adsorbent particles in water (Zetasizer Nano ZS, Malvern Instruments).

4.4. Adsorption Experiments. The adsorption experiments were carried out in batches under isothermal conditions (30 °C) in a thermostatic shaking water bath (Julabo SW23). Aqueous solution (100 mL) of AO-II of the known concentration taken in a 250 mL stoppered glass conical flask was contacted with a fixed amount of the adsorbent for a definite time period in the thermostatic shaking water bath. Thereafter, the solution was filtered and the residual dye concentration in the filtrate was determined spectrophotometrically (Cary 100 UV−Visible spectrophotometer, Agilent Technologies, USA) at 483 nm wavelength. The adsorption capacity was calculated using the formula

$$\text{Adsorption capacity, } q_e(mg/g) = \frac{(C_0 - C_e) \times v}{w \times 1000} \quad (7)$$

The percentage adsorption was calculated using the formula

$$\% \text{ Adsorption} = \frac{(C_0 - C_e) \times 100}{C_0} \quad (8)$$

where q_e is the amount of dye (AO-II) adsorbed per unit gram of the adsorbent at equilibrium, C_0 is the initial AO-II concentration, C_e is the equilibrium AO-II concentration (mg/L), v is the volume of AO-II solution in liter, and w is the weight of the adsorbent in grams.

On the basis of the adsorbent dose variation experiment presented in Figure S9, the adsorbent dose was kept at 0.5 g/L (84.9% adsorption) in all the batch adsorption experiments, so that the influence of various parameters (incremental or detrimental) can be detected. Except the adsorption isotherm experiments, all other adsorption studies were performed on an initial AO-II concentration of 200 mg/L.

Adsorption kinetics was studied for a time period of 0−6 h with an initial AO-II concentration of 100 and 200 mg/L. Sample solutions were withdrawn at fixed time intervals and measured for residual AO-II concentrations.

The adsorption isotherm experiments were performed at three different temperatures, 30, 40 and 50 °C, and the initial AO-II concentration was varied between 200 and 800 mg/L and the contact time was 2 h.

The desorption study was carried out using AO-II saturated LDH/PEG-15 for which 0.05 g of LDH/PEG-15 was contacted with 100 mL of 200 mg/L AO-II solution for 24 h. The AO-II saturated LDH/PEG-15 was separated and dried at 65 °C. The AO-II/LDH/PEG-15 thus obtained was then contacted with 100 mL water and the concentration of

DOI: 10.1021/acsomega.8b02743
ACS Omega 2019, 4, 3745−3754

desorbed AO-II in the solution was determined as a function of time. The percentage desorption was calculated with respect to the amount of AO-II loaded on the adsorbent. The same procedure was followed for desorption studies in 0.05 M NaOH solution.

To regenerate the used adsorbent, the AO-II loaded adsorbent was calcined at 480 °C for 1 h, cooled, and then treated with 15% aqueous solution of PEG_{400} for 4 h at 50 °C. Afterward, the adsorbent was separated by centrifugation and dried at 50 °C in an air oven.

To study the influence of pH on the AO-II uptake by the LDH/PEG composites, the initial pH values of the AO-II solutions were adjusted using dilute HCl/NaOH.

All the experiments were repeated three times, and the average values are reported.

■ ASSOCIATED CONTENT

Supporting Information

The Supporting Information is available free of charge on the ACS Publications website at DOI: 10.1021/acsomega.8b02743.

Nitrogen adsorption−desorption isotherms and the BJH desorption plots of pore volume versus pore diameter for PLDH and LDH/PEG-15; pseudo-second-order kinetic plots for the PLDH and LDH/PEG-15; influence of concentration variation on AO-II uptake at different reaction temperatures; van't Hoff plot for LDH/PEG-15; pH variation experiment for PLDH and LDH/PEG-15; particle size distribution of the PLDH, LDH/PEG-15 and LDH/PEG-50; and adsorbent dose variation for LDH/PEG-15 (PDF)

■ AUTHOR INFORMATION

Corresponding Author

*E-mail: sujata@clri.res.in, sujatamandal@rediffmail.com. Phone: +91 44 24437167. Fax: +82-63-270-4084.

ORCID

Sujata Mandal: 0000-0002-0549-8851

Asit Baran Mandal: 0000-0001-7953-941X

Present Address

§CSIR-Central Glass and Ceramic Research Institute, 196 Raja S. C. Mullick Road, Jadavpur, Kolkata 700032, India.

Notes

The authors declare no competing financial interest.

■ ACKNOWLEDGMENTS

Authors wish to acknowledge the financial support received from the Science and Engineering Research Board (SERB), Department of Science and Technology, Government of India (grant no. SR/FT/CS-145/2011). CSIR-CLRI Communication no. 1220. A.B.M. is also grateful to the Indian National Academy of Engineering (INAE) and CSIR-CGCRI, Kolkata for INAE Distinguished Professorship.

■ REFERENCES

(1) Joshi, M.; Purwar, R. Developments in new processes for colour removal from effluent. *Rev. Prog. Color. Relat. Top.* **2004**, *34*, 58−71.

(2) Fung, K. Y.; Lee, C. M.; Ng, K. M.; Wibowo, C.; Deng, Z.; Wei, C. Process development of treatment plants for dyeing wastewater. *AIChE J.* **2011**, *58*, 2726−2742.

(3) Ahmad, A.; Mohd-Setapar, S. H.; Chuong, C. S.; Khatoon, A.; Wani, W. A.; Kumar, R.; Rafatullah, M. Recent advances in new generation dye removal technologies: novel search for approaches to reprocess wastewater. *RSC Adv.* **2015**, *5*, 30801−30818.

(4) Yagub, M. T.; Sen, T. K.; Afroze, S.; Ang, H. M. Dye and its removal from aqueous solution by adsorption: A review. *Adv. Colloid Interface Sci.* **2014**, *209*, 172−184.

(5) Verma, A. K.; Dash, R. R.; Bhunia, P. A review on chemical coagulation/flocculation technologies for removal of colour from textile wastewaters. *J. Environ. Manage.* **2012**, *93*, 154−168.

(6) Asghar, A.; Raman, A. A. A.; Daud, W. M. A. W. Advanced oxidation processes for in-situ production of hydrogen peroxide/hydroxyl radical for textile wastewater treatment: a review. *J. Clean. Prod.* **2015**, *87*, 826−838.

(7) Yao, L.; Zhang, L.; Wang, R.; Chou, S.; Dong, Z. A new integrated approach for dye removal from wastewater by polyoxometalates functionalized membranes. *J. Hazard. Mater.* **2016**, *301*, 462−470.

(8) Paz, A.; Carballo, J.; Pérez, M. J.; Domínguez, J. M. Biological treatment of model dyes and textile wastewaters. *Chemosphere* **2017**, *181*, 168−177.

(9) Alatalo, S.-M.; Mäkilä, E.; Repo, E.; Heinonen, M.; Salonen, J.; Kukk, E.; Sillanpää, M.; Titirici, M.-M. Meso- and microporous soft templated hydrothermal carbons for dye removal from water. *Green Chem.* **2016**, *18*, 1137−1146.

(10) Kashif, U. M. A review on the adsorption of heavy metals by clay minerals, with special focus on the past decade. *Chem. Eng. J.* **2017**, *308*, 438−462.

(11) Ngulube, T.; Gumbo, J. R.; Masindi, V.; Maity, A. An update on synthetic dyes adsorption onto clay based minerals: A state-of-art review. *J. Environ. Manage.* **2017**, *191*, 35−57.

(12) Goldfarb, J. L.; Buessing, L.; Gunn, E.; Lever, M.; Billias, A.; Casoliba, E.; Schievano, A.; Adani, F. Novel Integrated Biorefinery for Olive Mill Waste Management: Utilization of Secondary Waste for Water Treatment. *ACS Sustainable Chem. Eng.* **2016**, *5*, 876−884.

(13) Gonçalves, J. O.; Silva, K. A.; Dotto, G. L.; Pinto, L. A. A. Adsorption Kinetics of Dyes in Single and Binary Systems Using Cyanoguanidine-Crosslinked Chitosan of Different Deacetylation Degrees. *J. Polym. Environ.* **2017**, *26*, 2401−2409.

(14) Gómez, P.-J.; Bringas, E.; Ortiz, I. Recent progress and future challenges on the use of high performance magnetic nano-adsorbents in environmental applications. *Chem. Eng. J.* **2014**, *256*, 187−204.

(15) Luo, J. Y.; Lin, Y. R.; Liang, B. W.; Li, Y. D.; Mo, X. W.; Zeng, Q. G. Controllable dye adsorption behavior on amorphous tungsten oxide nanosheet surfaces. *RSC Adv.* **2015**, *5*, 100898−100904.

(16) Haque, E.; Lo, V.; Minett, A. I.; Harris, A. T.; Church, T. L. Dichotomous adsorption behaviour of dyes on an amino-functionalised metal-organic framework, amino-MIL-101(Al). *J. Mater. Chem. A* **2014**, *2*, 193−203.

(17) Miyata, S. The Syntheses of Hydrotalcite-Like Compounds and Their Structures and Physico-Chemical Properties I: The Systems Mg2+-Al3+-NO3−, Mg2+-Al3+-Cl−, Mg2+-Al3+-ClO4−, Ni2+-Al3+-Cl− and Zn2+-Al3+-Cl−. *Clays Clay Miner.* **1975**, *23*, 369−375.

(18) Vaccari, A. Clays and catalysis: a promising future. *Appl. Clay Sci.* **1999**, *14*, 161−198.

(19) Drits, V. A.; Bookin, A. S. *Layered Double Hydroxides: Present and Future*; Rives, V., Ed.; Nova Science Publishers, Inc.: New York, 2001; p 39.

(20) Li, D.; Xu, X.; Xu, J.; Hou, W. Poly(ethylene glycol) haired layered double hydroxides as biocompatible nanovehicles: Morphology and dispersity study. *Colloids Surf., A* **2011**, *384*, 585−591.

(21) Leroux, F.; Besse, J.-P. Polymer Interleaved Layered Double Hydroxide: A New Emerging Class of Nanocomposites. *Chem. Mater.* **2001**, *13*, 3507−3515.

(22) Utracki, L. A.; Sepehr, M.; Boccaleri, E. Synthetic, layered nanoparticles for polymeric nanocomposites (PNCs). *Polym. Adv. Technol.* **2007**, *18*, 1−37.

(23) Yan, Z.; Zhu, B.; Yu, J.; Xu, Z. Effect of calcination on adsorption performance of Mg-Al layered double hydroxide prepared by a water-in-oil microemulsion method. *RSC Adv.* **2016**, *6*, 50128−50137.

DOI: 10.1021/acsomega.8b02743
ACS Omega 2019, 4, 3745−3754

(24) Yang, Q. Z.; Sun, D. J.; Zhang, C. G.; Wang, X. J.; Zhao, W. A. Synthesis and Characterization of Polyoxyethylene Sulfate Intercalated Mg−Al−Nitrate Layered Double Hydroxide. *Langmuir* **2003**, *19*, 5570−5574.
(25) Kumar, A. S. K.; Kalidhasan, S.; Rajesh, V.; Rajesh, N. Application of Cellulose-Clay Composite Biosorbent toward the Effective Adsorption and Removal of Chromium from Industrial Wastewater. *Ind. Eng. Chem. Res.* **2011**, *51*, 58−69.
(26) Ho, Y.; McKay, G. The kinetics of sorption of divalent metal ions onto sphagnum moss peat. *Water Res.* **2000**, *34*, 735−742.
(27) Darmograi, G.; Prelot, B.; Layrac, G.; Tichit, D.; Martin-Gassin, G.; Salles, F.; Zajac, J. Study of adsorption and intercalation of orange-type dyes into Mg-Al layered double hydroxide. *J. Phys. Chem. C* **2015**, *119*, 23388−23397.
(28) Langmuir, I. The adsorption of gases in plane surface of glass, mica, and platinum. *J. Am. Chem. Soc.* **1916**, *40*, 1361−1403.
(29) Freundlich, H. M. F. Over the adsorption in solution. *J. Phys. Chem.* **1906**, *57*, 385−471.
(30) Aharoni, C.; Sparks, D. L. *Kinetics of Soil Chemical Reaction: A Theoretical Treatment*; Sparks, D. L., Suarez, D. L., Eds.; Soil Science Society of America: Madison, WI, 1991; pp 1−18.
(31) Treybal, R. E. *Mass Transfer Operations*; McGraw-Hill: New York, 1981; p 590.
(32) Fahel, J.; Kim, S.; Durand, P.; André, E.; Carteret, C. Enhanced catalytic oxidation ability of ternary layered double hydroxides for organic pollutants degradation. *Dalton Trans.* **2016**, *45*, 8224−8235.
(33) Zhang, L.; Chen, L.; Liu, X.; Zhang, W. Effective removal of azo-dye orange II from aqueous solution by zirconium-based chitosan microcomposite adsorbent. *RSC Adv.* **2015**, *5*, 93840−93849.
(34) Marçal, L.; de Faria, E. H.; Saltarelli, M.; Calefi, P. S.; Nassar, E. J.; Ciuffi, K. J.; Trujillano, R.; Vicente, M. A.; Korili, S. A.; Gil, A. Amine-functionalized titanosilicates prepared by the sol-gel process as adsorbents of the azo-dye Orange-II. *Ind. Eng. Chem. Res.* **2011**, *50*, 239−246.
(35) He, C.; Hu, X. Anionic dye adsorption on chemically modified ordered mesoporous carbons. *Ind. Eng. Chem. Res.* **2011**, *50*, 14070−14083.
(36) Géraud, E.; Bouhent, M.; Derriche, Z.; Leroux, F.; Prévot, V.; Forano, C. Texture effect of layered double hydroxides on chemisorption of Orange II. *J. Phys. Chem. Solids* **2007**, *68*, 818−823.
(37) Li, K.; Zheng, Z.; Feng, J.; Zhang, J.; Luo, X.; Zhao, G.; Huang, X. Adsorption of p-nitroaniline from aqueous solutions onto activated carbon fiber prepared from cotton stalk. *J. Hazard. Mater.* **2009**, *166*, 1180−1185.
(38) Mandal, S.; Mayadevi, S.; Kulkarni, B. D. Adsorption of aqueous Selenite [Se(IV)] Species on Synthetic Layered Double Hydroxide Materials. *Ind. Eng. Chem. Res.* **2009**, *48*, 7893−7898.
(39) Mandal, S.; Natarajan, S.; Raja, S.; Vijayalakshmi, N.; Muralidharan, C.; Mandal, A. B. Adsorption of acid dyes on hydrotalcite-like anionic clays. *Key Eng. Mater.* **2013**, *571*, 57−69.
(40) Mandal, S.; Tichit, D.; Lerner, D. A.; Marcotte, N. Azoic Dye Hosted in Layered Double Hydroxide: Physicochemical Characterization of the Intercalated Materials. *Langmuir* **2009**, *25*, 10980−10986.
(41) Chiang, M.-F.; Wu, T.-M. Intercalation of γ-PGA in Mg/Al layered double hydroxides: An in situ WAXD and FTIR investigation. *Appl. Clay Sci.* **2011**, *51*, 330−334.
(42) Wang, C.; Zhang, X.; Xu, Z.; Sun, X.; Ma, Y. Ethylene Glycol Intercalated Cobalt/Nickel Layered Double Hydroxide Nanosheet Assemblies with Ultrahigh Specific Capacitance: Structural Design and Green Synthesis for Advanced Electrochemical Storage. *ACS Appl. Mater. Interfaces* **2015**, *7*, 19601−19610.
(43) Bourikas, K.; Stylidi, M.; Kondarides, D. I.; Verykios, X. E. Adsorption of Acid Orange 7 on the Surface of Titanium Dioxide†. *Langmuir* **2005**, *21*, 9222−9230.
(44) Grafov, A.; Leskala, M.; Grafova, I. Method of producing inorganic layered double hydroxides, novel inorganic layered double hydroxides and uses of the same. U.S. Patent US20,130,095,323 A1, April 18, 2013.
(45) Mandal, S.; Mayadevi, S. Adsorption of fluoride ions by Zn-Al layered double hydroxides. *Appl. Clay Sci.* **2008**, *40*, 54−62.
(46) Gunister, E.; Bozkurt, A. M.; Catalgil-Giz, H. Poly (diallyldimethylammoniumchloride)/sodium-montmorillonite composite; structure, and adsorption properties. *J. Appl. Polym. Sci.* **2013**, *129*, 1232−1237.

DOI: 10.1021/acsomega.8b02743
ACS Omega 2019, 4, 3745−3754